PEG-PGA enveloped octaarginine-peptide nanocomplexes: An oral peptide delivery strategy

Zhigao Niu, Eleni Samaridou, Emilie Jaumain, Julie Coëne, Gabriela Ullio, Neha Shrestha, Josep Garcia, Matilde Durán-Lobato, Sulay Tovar, Manuel J Santander-Ortega, et al.

Journal of Controlled Release 276 (2018) 125–139

Contents lists available at ScienceDirect

Journal of Controlled Release

journal homepage: www.elsevier.com/locate/jconrel

PEG-PGA enveloped octaarginine-peptide nanocomplexes: An oral peptide delivery strategy

Zhigao Niu[a,1], Eleni Samaridou[a,1], Emilie Jaumain[b], Julie Coëne[b], Gabriela Ullio[b], Neha Shrestha[c], Josep Garcia[d], Matilde Durán-Lobato[a], Sulay Tovar[e], Manuel J. Santander-Ortega[f,g], M. Victoria Lozano[f,g], M. Mar Arroyo-Jimenez[f,g], Rocío Ramos-Membrive[h], Iván Peñuelas[h], Aloïse Mabondzo[b], Véronique Préat[c], Meritxell Teixidó[d], Ernest Giralt[d], María José Alonso[a,*]

[a] Center for Research in Molecular Medicine and Chronic Diseases, IDIS research Institute, Department of Pharmacy and Pharmaceutical Technology, School of Pharmacy, University of Santiago de Compostela, 15782 Santiago de Compostela, Spain
[b] Service de Pharmacologie et d'Immunoanalyse, IBITECS, CEA, Université Paris-Saclay, F-91191 Gif-sur-Yvette, France
[c] Louvain Drug Research Institute, Advanced Drug Delivery and Biomaterials, Université Catholique de Louvain, B-1200 Brussels, Belgium
[d] Institute for Research in Biomedicine (IRB Barcelona), Barcelona Institute for Science and Technology (BIST), 08028 Barcelona, Spain
[e] Biomedical Research Group, Center for Research in Molecular Medicine and Chronic Diseases, University of Santiago de Compostela, 15782 Santiago de Compostela, Spain
[f] Cellular Neuroanatomy, Molecular Chemistry of Central Nervous System Group, Faculty of Pharmacy, University of Castilla-La Mancha, 02071 Albacete, Spain
[g] Regional Centre of Biomedical Research (CRIB), University of Castilla-La Mancha, Albacete, Spain
[h] Radiopharmacy Unit, Department of Nuclear Medicine, Clínica Universidad de Navarra, University Clinic of Navarra, 31008 Pamplona, Spain

ARTICLE INFO

Keywords:
Cell penetrating peptide
Octaarginine
PEGylation
Nanocomplex
Oral peptide/protein delivery

ABSTRACT

The objective of this work was the development of a new drug nanocarrier intended to overcome the barriers associated to the oral modality of administration and to assess its value for the systemic or local delivery of peptides. The nanocarrier was rationally designed taking into account the nature of the intestinal barriers and was loaded with insulin, which was selected as a model peptide. The nanocarrier consisted of a complex between insulin and a hydrophobically-modified cell penetrating peptide (CPP), enveloped by a protecting polymer. The selected CPP was octaarginine (r8), chemically conjugated with cholesterol (Chol) or lauric acid (C12), whereas the protecting polymer was poly (glutamic acid)-poly (ethylene glycol) (PGA-PEG). This enveloping material was intended to preserve the stability of the nanocomplex in the intestinal medium and facilitate its diffusion across the intestinal mucus. The enveloped nanocomplexes (ENCPs) exhibited a number of key features, namely (i) a unimodal size distribution with a mean size of 200 nm and a neutral zeta potential, (ii) the capacity to associate insulin (~100% association efficiency) and protect it from degradation in simulated intestinal fluids, (iii) the ability to diffuse through intestinal mucus and, most importantly, (iv) the capacity to interact with the Caco-2 model epithelium, resulting in a massive insulin cell uptake (47.59 ± 5.79%). This enhanced accumulation of insulin at the epithelial level was not translated into an enhanced insulin transport. In fact, only 2% of insulin was transported across the monolayer, and this was correlated with a moderate response of insulin following oral administration to healthy rats. Despite of this, the accumulation of the insulin-loaded nanocarriers in the intestinal mucosa could be verified *in vivo* upon their labeling with ^{99m}Tc. Overall, these data underline the capacity of the nanocarriers to overcome substantial barriers associated to the oral modality of administration and to facilitate the accumulation of the associated peptide at the intestinal level.

1. Introduction

The interest of pharmaceutical industry in developing therapeutic peptides and proteins has increased significantly over the last decades [1,2]. Unfortunately, the exploitation of these drugs has been limited by their difficult access to the target tissues. In general, peptide drugs

* Corresponding author.
E-mail address: mariaj.alonso@usc.es (M.J. Alonso).
[1] These authors contributed equally to this work.

https://doi.org/10.1016/j.jconrel.2018.03.004
Received 28 October 2017; Received in revised form 26 February 2018; Accepted 4 March 2018
Available online 06 March 2018
0168-3659/

intended to treat systemic diseases need to be administered by injection, a situation that hampers their utility in the case of a chronic pathology. On the other hand, peptides intended to act locally in the intestinal mucosa cannot be effectively used due to the difficulties for overcoming the stability and permeability barriers associated to the gastro-intestinal tract [3,4]. This situation has stimulated significant research in the drug delivery field. However, the inconclusive results reported until now and the limited number of oral peptide formulations in the market, or in clinical trials, have led to the conclusion that the development of oral peptide formulations represents a great challenge. The main delivery strategies explored so far have relied on the use of penetration enhancers or the association of the peptide to a nano-drug delivery carrier [5–7]. A particular category of penetration enhancers that has attracted significant attention is the so-called cell penetrating peptides (CPP). For example, Morishita and co-workers have shown the capacity of these molecules to promote the intestinal absorption of insulin [8,9]. On the other hand, since the pioneering work by Couvreur and co-workers [10,11] showing the possibility to deliver insulin in rats using polyacrylate nanocapsules, an array of nanocarriers including liposomes [12,13] as well as nanoparticles (NPs) made of chitosan [14–18], poly(lactic/glycolic) (PLGA) [19–21], acrylic polymers [22–24], and solid lipids [25,26] have been proposed for the oral administration of systemically acting peptide drugs. Similarly, nano/microparticles mainly relying on PLGA, chitosan and acrylic/methacrylic acid polymers (*i.e.* Eudragit®) have also been proposed for the oral administration of peptides/proteins acting locally in the intestinal mucosa [27–29]. Overall, these nanocarriers have led to variable results in terms of their capacity to enhance the systemic absorption of the associated peptide, or its retention at the level of the intestinal mucosa, and their progress towards advanced preclinical development phase has been scarcely reported. Indeed, currently there are only two oil-based nanoformulations, for the systemic delivery of cyclosporine, available in the market, whereas a few nano-based technologies for systemically acting peptide/protein drugs are under clinical development [6].

As a disruptive alternative to the technologies indicated above, here we present a new delivery strategy that involves a combination of key components with the appropriate architectural organization. The selection of the constituents and their organization was done in a rational manner, taking into account the biological barriers to be overcome [30–32]. More precisely, the novelty of our approach relies on the formation of nanocomplexes between the selected peptide and chemically modified CPPs, instead of their simple co-administration or conjugation, and the subsequent envelopment of these nanocomplexes with protective biopolymers. The selected model peptide was insulin, and the chosen CPP was r8 chemically modified with hydrocarbon chains in order to promote its interaction with insulin through electrostatic and hydrophobic forces. These nanocomplexes were enveloped with a biomaterial intended to prevent their interaction with digestive enzymes, *i.e.* pancreatin, and their subsequent aggregation and/or peptide degradation. For this purpose, we chose the copolymer polyglutamic acid-polyethylene glycol (PGA-PEG), with the assumption that the carboxylic moieties of the polyglutamic chain would interact with the cationic insulin-r8 complex, thereby protecting the nanocomplex and projecting the PEG molecule towards the external phase [33]. This PEG surface was also supposed to facilitate the diffusion of the complexed peptide across the intestinal mucus [34–36]. The nanostructures resulting from this rational design, here named as enveloped nanocomplexes (ENCPs), were characterized in terms of (i) their stability in simulated intestinal fluids (SIF), (ii) their ability to protect insulin from enzymatic degradation (*i.e.* by pancreatin), (iii) their mechanism of interaction with the intestinal epithelium, (iv) their ability to diffuse through intestinal mucus, (v) their biodistribution following oral administration and (vi) their potential for the systemic delivery of insulin in rats.

2. Materials and methodology

2.1. Materials

Recombinant human insulin monomer (Apidra®, Mw 5823 Da) was kindly provided by Sanofi (Paris, France). Fmoc-D-Arg(Pbf)-OH was purchased from Iris Biotech GmbH (Marktredwitz, Germany). Branch ($[PGA]_{100}$-m$[PEG]_6$ Poly(L-glutamic acid gamma- (omega-methoxyhepta (ethylene glycol))) sodium salt, 10–20 mol% mPEG substitution, MW = 22.8–24.7 kDa, 14–27% PEG) was purchased from Polypeptide Therapeutic Solutions (PTS, Valencia, Spain). Diblock (m$[PEG]_{455}$-b-$[PGA]_{10}$, methoxy-poly(ethylene glycol)-*block*-poly(L-glutamic acid sodium salt), MW = 22 kDa, 20 kDa PEG and 2 kDa PGA) was purchased from Alamanda Polymers (Huntsville, USA). Lauric acid, cholesteryl chloroformate, pancreatin (8xUSP), monobasic potassium phosphate, maleic acid, sodium chloride and sodium hydroxide were purchased from Sigma Aldrich (St. Louis, USA). Sodium taurocholate was purchased from New Zealand Pharmaceuticals (Palmerston North, New Zealand). Soy lecithin was purchased from Archer Daniels Midland (Chicaco, USA). Human colorectal adenocarcinoma Caco-2 cells (ATCC® HTB37™) were purchased from American Type Culture Collection (Manassas, VA, USA). High glucose Dulbecco's modified eagle medium (DMEM) and non-essential amino acid (NEAA) solution were purchased from Sigma Aldrich (St. Louis, USA), while heat inactivated fetal bovine serum (FBS), penicillin-streptomycin solution, L-glutamine, phosphate-buffered saline (PBS), Dulbecco's phosphate-buffered saline with calcium and magnesium (DPBS) were purchased from Lonza (Basel, Switzerland). Hank's balanced salt solution (HBSS), Rhodamine Phalloidin, Hoechst® 33342 were purchased from Life Technologies (USA). Phalloidin-iFluor 594 Reagent - CytoPainter (ab176757) was purchased from Abcam, UK. Fresh porcine intestinal mucus was obtained from the local slaughterhouse. ^{99}Mo-^{99m}Tc generator (Drytec; GE Healthcare Bio-science, UK) was eluted with 0.9% NaCl following the manufacturer's instructions. $SnCl_2{\cdot}2H_2O$ was purchased from Panreac (Barcelona, Spain); 0.9% NaCl was purchased from Braun. The anesthetic isoflurane (Isoflo™; Esteve, UK) and the euthanasic T-61 (Intevet, Spain) were used for the animals in biodistribution studies. Ultrapurified water was obtained from Millipore Milli-Q Plus water purification system (Darmstadt, Germany). All other chemicals were of analytical grade.

2.2. Synthesis of C12-r8 and cholesterol-r8

C12-r8 and Chol-r8 (Fig. S1) were synthesized by solid-phase peptide synthesis (SPPS) following the Fmoc/*t*Bu strategy. In both cases, Fmoc-Rink amide ChemMatrix® resin was used to obtain an amide group in the peptides *C*-terminus. TBTU and DIEA were used as coupling reagents for each amino acid incorporation (all amino acids were in the D-form). Fmoc deprotection was performed by the addition of 20% piperidine in DMF. Lauric acid and cholesteryl chloroformate were coupled to the *N*-terminus using the same strategy. Complete cleavage of both peptides from the resin and removal of the side-chain protecting groups were achieved by using the following cleavage cocktail: TFA/H_2O/TIS (95%/2.5%/2.5%). In the case of the FITC labelled C12-r8, introduction of a D-lysine, orthogonally protected, to the *C*-terminal of the peptides allowed the incorporation of 5(6)-Carboxyfluorescein (*CF*) to the peptide sequence. Once the peptide was synthesized, C12 was coupled to the *N*-terminal. Then, the Alloc protecting group was selectively removed from the D-lysine side chain by treatment with tetrakis (triphenylphosphine) palladium (0) followed by incorporation of *CF*, using standard amino acid coupling conditions. Both peptides were then purified by RP-HPLC at semi-preparative scale and characterized by HPLC (Waters Alliance 2695, photodiode array detector 2998 Waters, Sunfire C_{18} column (100 × 4.6 mm × 3.5 μm, 1 mL/min Acetonitrile (0.036% TFA) and H_2O (0.045% TFA). MALDI spectrometry (MALDI-TOF Applied Biosystem 4700, and 8-min linear gradients

were used in all cases. All peptides were obtained with a purity higher than 90%.

2.3. Preparation of r8-insulin nanocomplexes (NCPs)

C12-r8-insulin and Chol-r8-insulin NCPs were formed in aqueous solutions driven by both hydrophobic and ionic interactions [37–39]. Briefly, C12-r8 or Chol-r8 were dissolved in water at a concentration of 1 mg/mL, whereas insulin (Apidra®, Mw 5823 Da, Sanofi, France) was dissolved at a concentration of 1 mg/mL in basic media with different pH (0.001 N NaOH or 0.01 N NaOH). The complexes were formed instantly upon mixing the solutions under magnetic stirring at different r8: insulin ratios (1:1 to 8:1). Blank controls were prepared by adding a NaOH solution to a C12-r8 or Chol-r8 solution to confirm the absence of micelle formation. Additionally, a solution of non-hydrophobized r8 was used to form a complex with insulin, as previously reported in the literature [8,40]. The pH of all NCPs was finally adjusted to 7 with HCl. In case of fluorescent NCPs, FITC-labelled C12-r8 was used instead of the non-fluorescent formulations.

2.4. Preparation of PGA-PEG enveloped r8-insulin nanocomplexes (ENCPs)

The cationic NCPs were enveloped by different materials, *i.e.* negatively charged diblock or branch type PGA-PEGs (Diblock: m[PEG]455-b-[PGA]10, methoxy-poly(ethylene glycol)-*block*-poly(L-glutamic acid sodium salt), MW = 22 kDa, 20 kDa PEG and 2 kDa PGA, Alamanda Polymers, USA; Branched: $[PGA]_{100}$-m$[PEG]_6$ Poly(L-glutamic acid gamma- (omega-methoxyhepta (ethylene glycol)) sodium salt, 10–20 mol% mPEG substitution, MW = 22.8–24.7 kDa, 14–27% PEG, PTS, Spain), at insulin:PGA-PEG mass ratio 1:0.7 and 1:2 respectively, leading to the formation of ENCPs. Two different enveloping strategies were studied, namely: i.) simple incubation by adding PGA-PEG solutions to NCP suspensions and, ii.) the film hydration method. According to the second method, PGA-PEG polymers were dissolved in water and then the water was evaporated in a round flask under reduced pressure at 37 °C, leading to the formation of a thin film, followed by the addition of NCPs to the same flask and 10 min rotation at room temperature and atmospheric pressure. After the NCPs were enveloped with the film, the pH of the final ENCPs suspension was adjusted to 7 with HCl.

2.5. Physicochemical characterization and morphology of nanocomplexes (NCPs and ENCPs)

Particle size and PDI were determined by Dynamic Light Scattering (DLS) using a Malvern Zeta-Sizer (NanoZS, ZEN 3600, Malvern Instruments, Worcestershire, UK) fitted with a red laser light beam (λ = 632.8 nm). The Z-potential was calculated from the mean electrophoretic mobility values determined by Laser Doppler Anemometry (LDA) using the same device. The morphological analysis of the NCPs and ENCPs was carried out using transmission electron microscopy (TEM, CM12, Philips, Netherlands), where samples were stained with phosphotungstic acid (2%, w/v) solution and placed on cupper grids with Formvard® for TEM observation.

2.6. Determination of the association efficiency of insulin to the nanocomplexes (NCPs and ENCPs)

The association efficiency (AE) of insulin to NCPs and ENCPs was determined by both indirect and direct method following separation of the complexes from suspension media by centrifugation (Hettich, Universal 32R, Germany) at 15,000 *g* for 15 min at 15 °C and measuring the free insulin in the suspension media or directly measuring the insulin involved in the NCPs. For the indirect method, the aqueous supernatant was collected and the amount of free insulin in the supernatant was determined by reverse phase HPLC (Agilent, 1100 Series, USA), using a C18 column (Superspher® RP-18 end-capped). As mobile phases, a buffer of phosphoric acid and sodium perchlorate was mixed with acetonitrile at different ratios (93:7 as phase A and 43:57 as phase B, both at pH 2.3). The AE of insulin in the formulation was calculated taking into account the total insulin amount involved in the formulation, and the free insulin found in the supernatant. For the direct measurement, 500 μL of 0.01 N HCl and 100 μL of DMSO were added successively to the sediment containing the NCPs, by vortexing (VELP Scientifica, Italy). The solution was injected into the HPLC system and the AE was calculated dividing the insulin amount determined in the ENCP sediment by the total insulin amount involved in the formulation. The final loading was calculated by dividing the amount of insulin associated (AE x total insulin in the formulation) by the theoretical amount of all the materials involved in the formulation.

2.7. Stability of nanocomplexes (NCPs and ENCPs) in simulated intestinal media

The colloidal stability of the NCPs and ENCPs was assessed upon incubation in simulated intestinal medium (SIF, pH 6.8) and fasted-state simulated intestinal fluid (FaSSIF-V2, pH 6.5) [41,42] for up to 6 h at 37 °C with a horizontal shaking of 300 rpm. At different times (0, 0.5, 1, 3 and 6 h), a 50 μL sample of the incubation medium was withdrawn in order to analyze the particle size, PDI and derived Count Rate (dCR). The compositions of standard SIF and FaSSIF-V2 media are shown in Table S1 of the supporting information. Stability in simulated gastric fluid was not assessed since the formulations were to be enclosed in a gastro-resistant capsule before their oral administration.

2.8. Stability of PGA-PEG enveloped nanocomplexes (ENCPs) upon storage

The ENCP suspensions were stored at 4 °C, room temperature (around 20 °C) and 37 °C for up to 2 months. The measurements of the particle size, PDI and dCR were carried out as described above. Additionally, a lyophilization study of the ENCPs was done to assess the possibility of processing the ENCPs suspension as a powder. Trehalose (2%, w/v) was added to the ENCPs suspension (0.12%, w/v) prior to freeze-drying (~50 h cycle) to facilitate the posterior re-suspension. The stability of the freeze dried ENCPs under storage (at room temperature in a desiccator) and the stability in SIF was analyzed measuring their particle size, polydispersity, Z-potential, and derived count rate after reconstitution, using the methodologies described above. The insulin leakage in SIF was evaluated determining the free peptide in the suspension medium.

2.9. Stability of ENCPs-entrapped insulin against pancreatic enzyme degradation

To assess the capacity of the ENCPs to protect insulin from enzymatic degradation in the intestinal environment, a proteolysis study was performed by incubating ENCPs in SIF containing 1% (w/v) pancreatin (Sigma Aldrich, USA). A volume of 250 μL of the diblock PGA-PEG enveloped ENCPs was incubated with 250 μL of the proteolysis medium at 37 °C under 300 rpm horizontal shaking. At different time points, samples were transferred to cold tubes, containing 300 μL of 0.1 N HCl to quench the enzymatic proteolysis, and the insulin content was quantified by liquid chromatography-mass spectrometry (LC-MS, (Shimadzu HPLC system LC 20AD, Japan; Thermo Triple quadrupole mass spectrometer Quantum Ultra, USA). The study was done in 3 replicates, and, as control, plain insulin solution instead of the ENCPs was treated with the same proteolysis medium. To exclude the interference of the pancreatin in the LC-MS analysis, the proteolysis medium alone was also set as an additional control.

2.10. In vitro release of insulin from nanocomplexes (NCPs and ENCPs)

The *in vitro* release study of C12-r8-insulin NCPs and the corresponding ENCPs was carried out in SIF, FaSSIF-V2 or acetate buffer (pH 4.0, 100 mM) at 37 °C. Briefly, the formulation was diluted in 10 mL of the corresponding media to a final insulin concentration 0.05 mg/mL. The formulations were placed at 37 °C in an incubator with 300 rpm horizontal shaking for 6 h, and during this time 500 μL samples were withdrawn at predetermined time points (0, 0.5, 1, 2, 4 and 6 h) and centrifuged at 15,000 g for 15 min at 15 °C. The same volume of the corresponding medium was added to replenish the release medium at each time point. The supernatant was collected for insulin determination by HPLC as described above.

2.11. Transport of PGA-PEG enveloped nanocomplexes (ENCPs) in intestinal mucus

The ability of the PGA-PEG enveloped nanocomplexes to move through intestinal mucus was assessed by particle tracking analysis as described elsewhere [43]. Fresh porcine intestinal mucus, obtained from the local slaughterhouse, was used as model of the intestinal mucus. FITC labelled ENCPs were employed throughout this study. Fluorescently labelled polystyrene NPs and PF-127 coated polystyrene NPs were used as the mucoadhesive control and the mucodiffusive control, respectively. Briefly, 3 μL of the FITC labelled ENCPs (1.2 mg/mL) or the fluorescently labelled control nanoparticles, previously diluted in MQ water, were mixed with 100 μL of mucus. Ten microliters of each mucus-nanoparticle mixture was placed between a microscope slide and a cover glass in a chamber created by a double-sided adhesive sticker of 120 μm thickness in between. The Nikon microscope equipped with a sCMOS camera and a PLAN APO 100× 1.4 oil-immersion objective was always focused at 10–15 μm above the coverglass. For each sample, 20–30 movies of 800 frames were recorded at a frame rate of 100 fps, obtaining > 200 trajectories per sample. The diffusion coefficient of each particle was obtained from the dependence of the mean square displacement (MSD), calculated as $MSD = [x(t + \tau) - x(t_0)]^2 + [y(t + \tau) - y(t_0)]^2$ [44], with the time as follows:

$$MSD = 4D_{eff}\tau^{\alpha}$$

where D_{eff} is the effective diffusion coefficient, τ the time scale or time lag and α is a parameter that provides information about the nature of the diffusion of the nanoparticle in the mucus. The parameter α was calculated as the slope of the MSD *vs.* τ plot; when the value of α is equal to 1, it indicates a free diffusion, whereas a decrease of this parameter down to 0.2 indicates that the diffusion is highly restricted [45–47].

2.12. Cytotoxicity on Caco-2 cells

Cytotoxicity was determined in Caco-2 cells (ATCC® HTB37™, American Type Culture Collection, USA) using a MTS assay as an indicator of cell viability according to the manufacturer's instructions for 96-microwell plates. Cell viability was assessed after the co-incubation of 10,000 Caco-2 cells/well on a 96-well tissue cultured plate (Corning® Costar®, USA) with the tested samples. For the MTS test, microplates were transferred to a humidified incubator at 37 °C with 5% CO_2 for a 2 h incubation. The supernatant of each well was then removed and the cells were rinsed with PBS and incubated with 100 μL of 3-(4,5-dimethylthiazol-2-yl)-5-(3-carboxymethoxyphenyl)-2-(4-sulfophenyl)-2H-tetrazolium (MTS) reagent at 37 °C for 2.5 h in a humidified atmosphere containing 5% CO_2. Cellular supernatants were then transferred into a new 96-well plate and the amount of soluble formazan produced by cellular reduction of MTS was determined by recording absorbance at 490 nm with a Synergy 4 microplate reader (BioTek Instruments, Inc., Winooski, USA).

2.13. Measurement of the transepithelial electrical resistance (TEER)

Caco-2 cell monolayers were cultured on the tissue-cultured-treated PET filter (diameter 1 μm, 1.1 cm^2) in Millipore Transwell® 12 wells/plates and were used for transport experiments 21 days after seeding. The C12-r8 based NCPs, diblock PGA-PEG enveloped C12-r8 ENCPs and the physical mixture of r8 and insulin were evaluated regarding their effect on the tightness of the cell monolayers, measuring the change of TEER in Caco-2 cell monolayers with a Millicell-Electrical Resistance System (Endohm-12, Millipore Corp). Monolayers with TEER values in the range of 800–1500 Ω/cm^2 were used, and all the groups were designed so as to have the same insulin concentration.

2.14. Quantitative cell uptake and transport of insulin

In parallel with the TEER measurement, the C12-r8 based NCPs, diblock PGA-PEG enveloped ENCPs and a physical mixture of insulin and r8 were evaluated in respect of the cell uptake/transport efficiency of insulin. After 2 h' incubation, on Caco-2 monolayer, samples were collected (500 μL) from the receiver compartment and the apical compartment, and insulin concentrations were measured using liquid chromatography - mass spectrometry. Cell monolayer was washed extensively in 0.9% NaCl and frozen at −80 °C for insulin quantification within the cells. Liquid chromatography with a 150 × 2.1 mm - 5 μm - 300 Å HPLC C8 column (Interchim, France) was used for elution of insulin in a gradient mode with mobile phases A and B, where solvent A was H_2O containing 0.1% formic acid and solvent B was acetonitrile containing 0.1% formic acid; the flow rate was 0.6 mL/min to avoid pressure rise. An aliquot (100 μL) of the sample was treated with 200 μL of chloroform/methanol/water at 1/1/0.3 and 100 μL of 0.1 M NaOH, and then 40 μL of analyte was injected onto the column placed in an oven at 60 °C. The total run time was 13 min. Detection was done by tandem mass spectrometry (Quantum Ultra) in positive electrospray mode. The limit of detection is 0.005 μg insulin. System control and data processing were carried out using MassLynx software version 4.1. Spray voltage was 3.0 kV, and sheath and auxiliary gas pressures were 50 and 15 (arbitrary units), respectively. The in-source CID energy was fixed at 12 V, and capillary temperature was 350 °C. Tube lens and collision energy values were optimized for insulin. Multiple reaction monitoring was used for the detection of the ion transitions. The multiple reaction monitoring transitions for analytes were as follows: *m/z* insulin 890.56 > 984.55, *m/z* insulin 1284.73 > 1104.60. Analytes were quantified by means of calibration curves using insulin as internal standard. The significance of differences in the mean values of different groups is evaluated using ANOVA between treatment groups followed by Tuke's multiple comparison *post hoc* test (SigmaPlot SyStat Software Inc., San Joes, CA). The standard curves showed linearity for creatine over a range of 0.025–10 μg/mL for insulin. The methodology for this assay involves reduction with dithiolthreitol 45 mM and alkylation with 100 mM of iodoacetamide 100 mM of intact insulin for measurement of the free B chain.

2.15. Interaction of PGA-PEG enveloped nanocomplexes (ENCPs) with Caco-2 cells

The interaction of a selected prototype consisting of C12-r8, insulin and diblock PGA-PEG with Caco-2 cells was studied by confocal laser scanning microscopy (CLSM), and the entrance of ENCPs into the cells was quantified by flow cytometry (FACS) after confirming the colloidal stability of FITC-labelled (λ_{em} = 519 nm) ENCPs and the absence of fluorescence leakage in relevant medium (HBSS). Caco-2 cells were seeded in 24-well cell culture plates at a density of 5×10^5 cells per well, allowed to adhere for 48 h until confluency, and then incubated with 400 μL of FITC-labelled ENCP (0.2 mg/mL) suspension in HBSS. After 2 h, cells were washed three times with PBS and detached from the plates by trypsinization. After a 10-min centrifugation at 1500 g

(Eppendorf centrifuge 5804 R, Daigger scientific Inc., USA), the supernatant was discarded, while the cells were resuspended in PBS and their FITC fluorescence quantified using a BD FACSVerse™ flow cytometer (Becton Dickinson Biosciences, San Jose, CA, US). For the CLSM study, experiments were preformed according to two experimental protocols. In one of them, the Transwell® inserts fixed in PFA 4% were gently washed in HBSS. Actin was stained with 200 μL of rhodamine-phalloidine (1:50) in buffered HBSS + 0.2% (v/v) Triton X-100 for 10 min in the dark to reveal cell borders, cell nuclei was stained with DAPI (1:20). Subsequently, inserts were washed in HBSS, cut and mounted on glass slides. Images were captured using a Zeiss™ confocal microscope (LSM 150). Data were analyzed by the Axio Vision software (*vs* 4.8) to obtain y-z, x-z and x-y views of the cells monolayers. In another experimental protocol, 200 μL of Caco-2 cells suspension were seeded at a concentration of 2×10^5 cells mL^{-1} in μ-Slide 8 well (Ibidi, Germany), previously coated with Poly-D-lysine hydrobromide (0.1 mg/mL), and allowed to adhere for 24 h, before gently washed twice in pre-warmed HBSS. Then, 200 μL of FITC-labelled ENCP suspension in HBSS at a concentration of 0.2 mg/mL were added to each chamber and incubated for 2 h at 37 °C. Cells were fixed with PFA 4% in HBSS for 20 min and washed twice with HBSS. Permeabilization step was performed adding buffered HBSS + 0.1% (v/v) Triton X-100 for 3 min and then washed with HBSS. Actin was stained with Phalloidin-iFluor 594 Reagent - CytoPainter (ab176757) 1× in HBSS +1% (w/v) BSA. Staining of cell nuclei was carried out simultaneously using Hoechst® 33342 (1:4000) for 30 min in the dark. Images were captured using a Leica TCS SP5 confocal microscope and data were analyzed by the Leica Application Suite software.

2.16. Labeling of PGA-PEG enveloped nanocomplexes (ENCPs) with Technetium-99m

Diblock PGA-PEG-coated ENCPs were labelled with Technetium-99m (^{99m}Tc) by the stannous chloride method [48], taking advantage of the functional groups on the surface of the carrier. As a first step, technetium was reduced to the 5^+ state with stannous chloride. The reduced ^{99m}Tc species formed then ionic/coordination bonds with the carboxylic acid groups (−COO−) of the PGA and/or the hydroxylic (−OH) groups of the PEG on the surface of the enveloped nanocomplexes. Briefly, 0.1 mL of previously prepared diblock PGA-PEG coated ENCPs at a concentration of 13.5 mg/mL were mixed with 0.04 mL of stannous chloride solution (0.05 mg/mL) in acidified water (pH adjusted to 4 with 0.1 N HCl), followed by the addition of 1.5 mCi of freshly eluted ^{99m}Tc-Pertecnetate ($^{99m}TcO_4^-$) in 0.1 mL NaCl 0.9%, which were then added to pre-reduced tin. The mixture was incubated at room temperature for 30 min with occasional gentle stirring. The overall procedure was carried out in helium-purged vials using helium-purged solutions to minimise oxygen content and avoid oxidation of pre-reduced tin. The efficiency of the labelling process was then assessed by an instant paper chromatography system with Whatman™ 3MM paper (Cellulose 0.34 mm; General Electric, Boston, Massachusetts, United States). The Whatman™ 3MM strip was spotted with the labelled complex and developed using NaCl 0.9%. Whatman 3MM strips were read using a MiniGita radiochromatographic system equipped with a 2 × 2 NaI (Tl) detector and MiniGita software (Raytest GmbH, Dortmund, Germany). The particle size and polydispersion of the labelled nanocomplexes were determined by photon correlation spectroscopy. Prior to the *in vivo* biodistribution studies, the stability of the radiolabeled ENCPs as well as the release of the radioisotope was evaluated in biorelevant media (Simulated gastric fluid (SGF, pH 4.0) and Simulated intestinal fluid (SIF, pH 6.8) without enzymes) simulating the *in vivo* condition in fasted rats.

2.17. In vivo biodistribution of radiolabeled PGA-PEG enveloped nanocomplexes (ENCPs)

The biodistribution of ^{99m}Tc-ENCPs was studied in male Wistar rats (n = 3) weighing 250–300 g that had been fasted for 12 h. One single dose of radiolabeled ENCPs, corresponding to 50 IU insulin/kg and 1 mCis of radioactivity/kg, was administered to each animal by oral gavage. Free ^{99m}Tc was also administered at the same dose (1 mCis/kg) as a control (n = 3). The animals were then anaesthetized with 1.5% isoflurane gas (in 100% oxygen) and placed in supine position on the SPECT–CT (Symbia; Siemens Medical System, USA). A high resolution low-energy parallel-hole collimator was used. SPECT images were obtained at predetermined time points (1, 2, 4, 6, 8, 26 h after administration), over a 360° arc, using 64 frames at 20 s per frame in a no circular orbit. The scan parameters for CT were 130 kV, 30 mAs, 1 mm slices and Flash 3D iterative reconstruction with a Gaussian filter with a full-width at half maximum of 8.4. Animals remained anaesthetized for the duration of the study. For quantification, the images were processed with the WorkflowEngine software and studies were exported to the PMOD software (version 3.0; Adlisvil, Switzerland) and covert to analyze format. Volumes of interest (VOIs) were drawn and evaluated in the SPECT-CT images to get the time-course evolution of the biodistribution of the labelled nanoparticles.

2.18. In vivo response to insulin-loaded ENCPs

Male Sprague-Dawley rats (240–300 g) were provided by the Central Animals House of the University of Santiago de Compostela. All animal experiments were reviewed and approved by the ethics committee of the University of Santiago de Compostela (procedures Prof. Carlos diéguez, 1500AE/12/FUN01/FIS02/CDG3) according to the European and Spanish regulations for the use of animals in animal studies; performed therefore in compliance with the Directive 2010/63 / EU of the European Parliament and Council of 22nd September 2010 on the protection of animals used for scientific purposes; Spain Royal Decree 1201/2005, of October 10th, on the protection of animals used for experimental and other scientific purposes and under the Royal Decree 296/2008 of Spain 30th December on the protection of animals used for experimental and other scientific purposes including teaching. The animals were kept under 12 h light/12 h dark cycles and were fed a standard laboratory rodent diet in pellets (Panlab A04, Panlab laboratories). They were fasted for 4 h before experiments (free access to water), and maintained conscious during the experiment. The animals' glucose level was tested right before starting the experiments and only those with blood glucose over 65 mg/dL were selected for the study. Oral administration of the insulin-loaded ENCPs (dosage 50 IU/kg) was performed by using an enteric capsule made of Eudragit® L100. As control, non-formulated insulin was incorporated into the enteric capsules and administered to animals following the same procedure (50 IU/kg). Blood samples were collected from the rat tail vein 30 min prior to the administration to establish the baseline blood glucose level. At time point 1, 2, 3, 4, 5, 6, 7, 8, 9 10 and 11 h after dosing, 0.1 mL of the blood samples were collected to determine the glucose level change, using a glucometer (Glucocard™ G+ meter, Arkray Factory, Japan). The statistical analysis was carried out using a Student's *t*-test. Differences were considered statistically significant at $^*p < 0.05$.

3. Results and discussion

The main objective of this study was the rational design of a nanocarrier intended to help peptides to overcome the biological barriers associated with the oral administration route. This design involved the formation of core-shell nanoparticles, where the nanoparticles core contained a modified CPP complexed to insulin and, the shell, made of PGA-PEG, had a protective role against the harsh intestinal environment. Our selection of r8 was based on its reported capacity to enhance

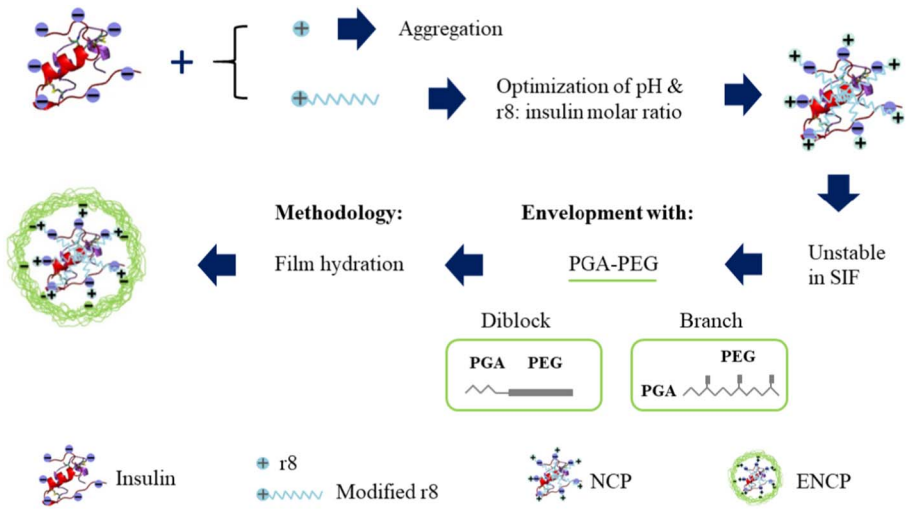

Fig. 1. Flow diagram showing the process for the rational design of ENCPs.

insulin absorption [40,49]. However, while in these previous studies, CPPs were simply mixed with insulin in solution [50], in this work we formed well-defined and uniform nanometric r8-insulin complexes. For this purpose, we synthesized hydrophobically modified r8, which would enable the formation of nanocomplexes through ionic and hydrophobic forces. The selection of the protective envelope was based on the reported capacity of PEGylated polymers to prevent nanoparticles aggregation [33] and enhance mucodiffusion [34]. Fig. 1 summarizes the process of the rational design of our nanosystems.

3.1. Development and physicochemical characterization of modified r8-insulin nanocomplexes (NCPs)

Two different amphiphilic r8 derivatives, cholesterol-r8 and lauric acid-r8, were synthesized to form insulin-CPP nanocomplexes (NCPs), with the idea of exploring the role of the hydrophobic moiety in the formation of well-defined and stable nanocomplexes. The non-modified r8 was also used as a control. In a first stage, and to favor the complexation, we dissolved insulin in basic media (0.001 N or 0.01 N NaOH) and r8 in water, before mixing both components in a 1:1 M ratio. As expected, the most basic pH (0.01 N NaOH), where the insulin molecules were negatively charged, led to the highest complexation efficiency with the r8 molecules. In a second stage, we studied the effect of the r8: insulin molar ratio on the nanocomplexes properties (Fig. 2). In the case of the non-modified r8, a r8: insulin molar ratio 1:1 (~400 nm) resulted in a very low insulin association (~10%, Fig. 2A), a result that suggests that the number of r8 molecules available for the ionic complexation of insulin was insufficient. As expected, by raising the r8: insulin molar ratio, the AE increased significantly and this led to the neutralization of the Z-potential (2B). However, the size of the complexes becomes too large and highly variable (2C), a result that could be attributed to the limited electrostatic repulsion between them (zeta potential close to 0).

On the other hand, as shown in Fig. 2, the capacity of C12-r8 or cholesterol-r8 to complex insulin was drastically different to that of the non-modified r8. At the r8: insulin molar ratio of 1:1, both NCP had a nanometric size (200–500 nm), a negative surface charge and a modest insulin association efficiency (AE: 60–70%). As the amount of modified-r8 increased, a neutralization of Z-potential value was observed at molar ratios between 2:1 to 3:1 for modified r8 and between 3:1 to 4:1 for non-modified r8 (2B). At these ratios, almost all insulin molecules were complexed with the CPP (~100% insulin AE) (2A). However, under these conditions, the lack of electrostatic repulsion between the particles, led to the formation of large aggregates. Subsequently, after the threshold of modified r8: insulin molar ratio 4:1, the surface charge of the NCPs became positive enough to prevent their aggregation [51], while the insulin AE remained 100%. The Z-potential of Cholesterol-r8-insulin and C12-r8-insulin NCPs reached a plateau at r8: insulin molar ratios of 5:1 and 8:1, respectively, indicating the saturation of the complexation process. Hence, these molar ratios were selected for the subsequent engineering of the nanocarriers. Overall, these results indicate that, as expected, the ionic interaction is not the only driving force in the complex formation and that the hydrophobic interactions between C12 chain or Cholesterol and insulin also play a significant role [52]. This situation is different from the one observed by other authors exploring the interaction of modified r8 with polynucleotides, based either on their covalent conjugation, or their complexation, solely driven by ionic forces [53–56]. Furthermore, these reported r8-polynucleotides complexes were not designed to be enveloped by a protecting polymer shell, as described in the following section.

3.2. Development and physicochemical characterization of ENCPs

Based on the results described above, we selected specific nanocomplexes compositions for their subsequent optimization. The optimization process was based on the premise that the positive surface charge of r8-insulin NCPs might have undesirable consequences, *i.e.* promote their interaction with negatively charged pancreatic enzymes and hamper their mucodiffusion [35,57]. In order to deal with these barriers, our approach was to envelop the NCPs with PEG derivatives. Though PEG presents a neutral charge, the steric hindrance provided by this polymer is well known for stability improvement [33,58]. For this purpose, in a first stage, we explored different non-ionic stabilizers, *i.e.* poloxamers or PEG stearate, as well as anionic derivatives, *i.e.* PGA-PEG. The analysis of the zeta potential values led us to the conclusion that the non-ionic polymers could not be attached to the surface of the NCPs. In contrast, when we used PGA-PEG, we observed the reversion of Z-potential of the NCPs from positive to negative, a result that made evident the success of the enveloping process (Fig. 3). We attributed the benefit of this polymer to its negative charge, which enable an adequate interaction with the positively charged nanocomplexes. In order to have a better understanding of the enveloping process, we used diblock PGA-PEG and branched PGA-PEG (Fig. 3) and applied two different methodologies: i) simple incubation and ii) film hydration.

Fig. 3 shows the characteristics of the ENCPs formed using the two methodologies and the two enveloping polymers, the diblock or branched PGA-PEG (NCPs consisting of C12-r8: insulin molar ratio 8:1). The results obtained with the incubation method indicate that for the diblock PGA-PEG, the association of insulin to the NCPs was maintained (Fig. 3A) and the positive charge was reduced (Fig. 3B). In contrast,

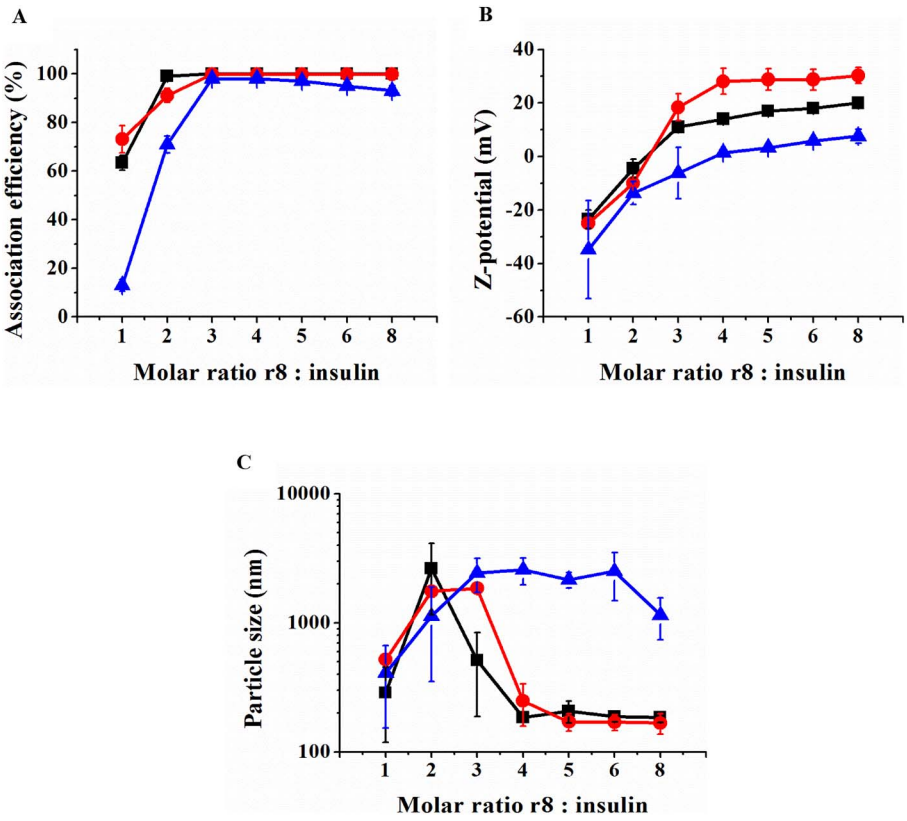

Fig. 2. (A) Association efficiency, (B) Z-potential, (C) particle size of non-coated C12-r8-insulin (black squares), Chol-r8-insulin complexes (red circles) and r8-insulin controls (blue triangles) at r8: insulin molar ratio from 1:1 to 8:1. Data are expressed as mean ± SD, n = 3. (For interpretation of the references to color in this figure legend, the reader is referred to the web version of this article.)

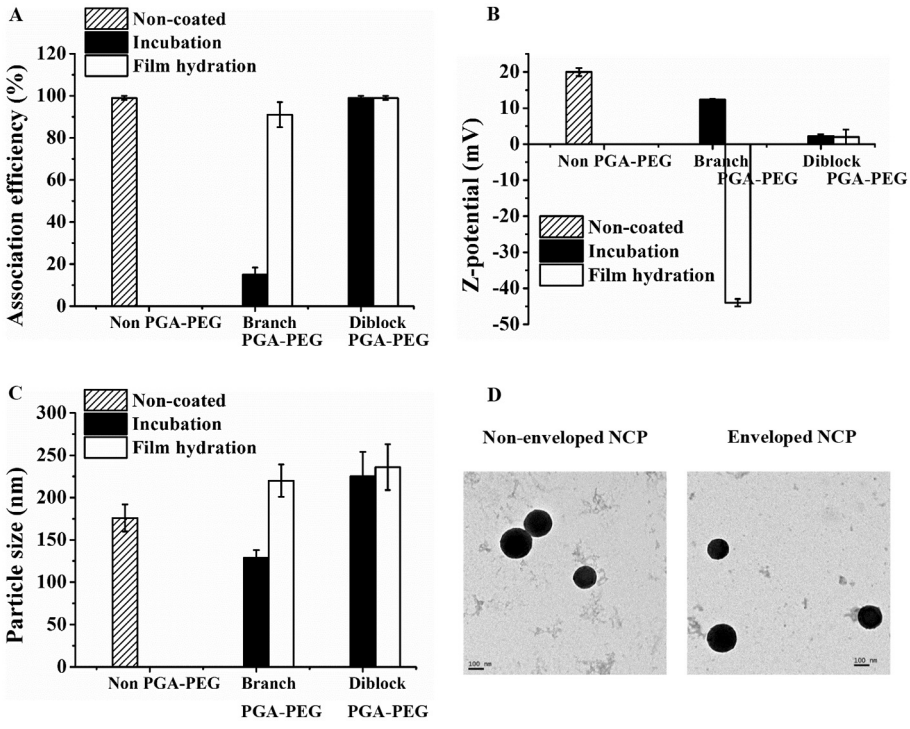

Fig. 3. (A) Peptide association efficiency, (B) Z-potential and (C) particle size of the non-enveloped C12-r8-insulin NCPs and those ENCPs coated by branched and diblock PGA-PEG polymers with different methods, data are expressed as mean ± SD, n > 10 for diblock PGA-PEG ENCPs, and n = 3 for the rest, and (D) TEM images of non-enveloped and diblock PGA-PEG enveloped C12-r8-insulin ENCPs.

when the enveloping polymer was the branched PGA-PEG, an important displacement of insulin (AE reduced from 100% to 15%), accompanied with an inversion of the zeta potential was observed. The different behavior of these two enveloping materials was explained on the basis of their chemical structure. The branched copolymer has an important negative charge attributed to the PGA (100 monomer units) and small 0.3 kDa PEG chains pending, whereas the diblock copolymer has 10 units of PGA, linked as a diblock to 20 kDa long PEG chains.

Table 1
Physicochemical properties, insulin association efficiency and final drug loading of non-enveloped C12-r8-insulin/Chol-r8-insulin NCPs and those ENCPs enveloped by diblock or branched PGA-PEG polymers using film hydration method. Data are expressed as mean ± SD, n > 10 for NCP and ENCP with C12-r8-insulin core, n = 3 for those with Chol-r8-insulin core.

NCP core	ENCP shell	Size (nm)	PDI	Z-pot (mV)	AE (%)	Loading (%)
C12-r8-insulin (r8: insulin 8:1)	Non-enveloped	176 ± 16	0.1	+20 ± 1	100 ± 0	33.3 ± 0
	Branch PGA-PEG	220 ± 19	0.1	−44 ± 1	91 ± 6	18.2 ± 1.2
	Diblock PGA-PEG	236 ± 27	0.1	+2 ± 2	99 ± 0	26.6 ± 0
Chol-r8-insulin (r8:insulin 5:1)	Non-enveloped	171 ± 26	0.1	+29 ± 4	100 ± 0	40.8 ± 0
	Branch PGA-PEG	202 ± 28	0.2	−43 ± 1	81 ± 4	18.2 ± 0.9
	Diblock PGA-PEG	225 ± 10	0.2	+2 ± 3	92 ± 9	26.8 ± 2.6

Thus, the large negative branched co-polymer molecules could have displaced insulin from the complexes, whereas the small PGA segment of the diblock copolymer, could be better accommodated around the positive nanocomplexes.

Unlike the incubation method, the film hydration method allowed the efficient accommodation of both types of PGA-PEG onto the surface of the cationic NCPs without impairing the AE of insulin (Fig. 3A). The surface charge of the NCPs changed from positive to neutral or negative values due to the attachment of the diblock or branched PGA-PEG, respectively (Fig. 3B). This could be attributed to the fact that the film hydration method allows for a gradual and more effective envelopment of the NCPs with the PGA-PEG molecules.

In order to confirm that the enveloping process did not alter the particle size and morphology of the particles, both NCPs and ENCPs were observed by TEM. Fig. 3D shows the images of C12-r8-insulin NCPs and their diblock PGA-PEG enveloped ENCPs. In agreement with the data obtained by DLS, the size and appearance of the nanocomplexes with or without envelope are very similar. Overall, the physicochemical properties and insulin complexation capacity observed for the selected NCPs and ENCPs are summarized in Table 1. To further assess the efficiency of the enveloping process, the stability of the ENCPs was evaluated as described in the next section.

3.3. Stability of ENCPs in simulated intestinal media

The colloidal stability of the nanocomplexes was tested in simulated intestinal media (SIF). As expected, considering their positive charge, the stability studies revealed that the non-enveloped NCPs aggregated massively. In contrast, the ENCPs enveloped with, either diblock or branch PGA-PEG exhibited an adequate colloidal stability in SIF for up to at least 4 h (see supporting information Fig. S2). However, when the ENCPs were incubated in a complex intestinal medium, *i.e.* FaSSIF-V2 medium, they showed a different behavior depending on the enveloping polymer. Indeed, while the diblock PGA-PEG ENCPs formulations remained stable for at least 6 h (Fig. 4), those enveloped by the branched PGA-PEG aggregated significantly. Based on the improved stability of the diblock PGA-PEG enveloped ENCPs under bio-relevant conditions, this system was selected as the basis for most of the subsequent studies described below.

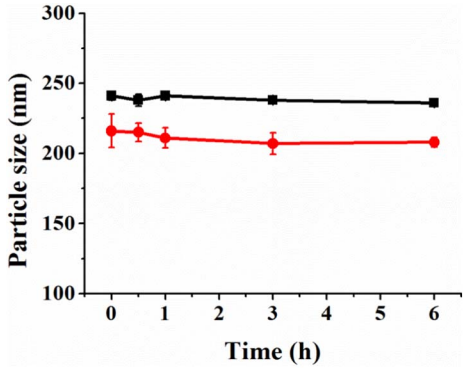

Fig. 4. The evolution of particle size of the diblock PGA-PEG enveloped C12-r8-insulin (black square) and Cholesterol-r8-insulin (red circle) ENCPs in FaSSIF-V2, respectively. (For interpretation of the references to color in this figure legend, the reader is referred to the web version of this article.)

3.4. Stability of ENCPs during storage and development of a freeze-dried formulation

The particle size of the C12-r8-insulin and Cholesterol-r8-insulin ENCPs formulated with diblock PGA-PEG was analyzed upon storage at 4 °C, at room temperature, and at 37 °C for up to 60 days. The C12-r8-insulin ENCPs presented the same characteristics after being stored for 2 months under the conditions shown above, while a decrease in dCR, indicative of a alteration in the concentration of the sample, was observed for the Chol-r8-insulin ENCPs at 4 °C and 37 °C after 30 days (see supporting information Fig. S3). In addition, the C12-r8-insulin enveloped with diblock PGA-PEG could be freeze-dried (in the presence of 2% trehalose) and reconstituted without altering their physicochemical properties (particle size and zeta potential, as well as the insulin AE, which remained to be 100%, leading to a drug loading of 27% (w/v)). Moreover, the stability of this dried product was maintained for at least 2 months upon storage at room temperature. The reconstitution of the dried product led to a suspension of ENCPs with a particle size of 210 nm (Fig. S4), a low PDI below 0.1, and a Z-potential around +1 mV. When exposed to SIF, the freeze-dried formulation (after up to 1-month storage) remained stable for at least 4 h without a significant peptide leakage (< 10%). The evolution of particle size is shown in Fig. S5. The dCR remained stable for the duration of the study and the PDI was below 0.1 in all cases. This possibility to convert the liquid suspension into a powder is particularly useful for the development of an oral formulation. Based on these results, the diblock PGA-PEG C12-r8-insulin ENCPs was selected as an adequate prototype for most of the subsequent studies described in the next sections.

3.5. Protection of insulin against enzymatic degradation

To assess the nanocarrier's ability to protect insulin against enzymatic degradation in the GIT tract, a proteolysis study of the diblock PGA-PEG enveloped C12-r8-insulin ENCPs was performed in SIF media including 1% (w/v) pancreatin (8 USP). The results revealed that after 15 min incubation in this drastic proteolysis medium, plain insulin was totally degraded. In contrast, the ENCPs efficiently protected the entrapped insulin from degradation (75.6 ± 8.8% remaining), and a significant amount of insulin (25.3 ± 4.6%) was still active after a 2-h incubation in the proteolytic medium (Fig. 5). Taking into account that pancreatin is mainly present in the duodenum region, and that the ENCPs are supposed to travel and be retained in different parts of the intestine, these results suggest that insulin may survive in the harsh intestinal ambient when is incorporated into the diblock PGA-PEG enveloped C12-r8-insulin ENCPs.

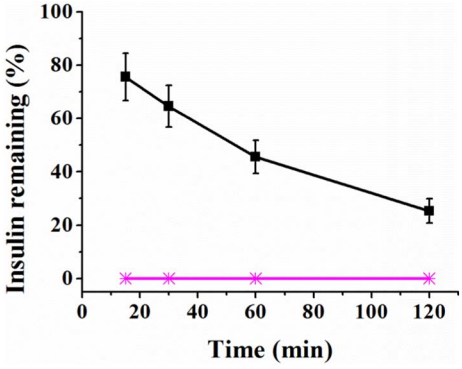

Fig. 5. The proteolysis study of diblock PGA-PEG enveloped C12-r8-insulin ENCPs (black square) and plain insulin solution (pink star) incubated in 1% (w/v) pancreatin (8 USP) supplemented SIF media. Data are expressed as mean ± SD, n = 3. (For interpretation of the references to color in this figure legend, the reader is referred to the web version of this article.)

3.6. In vitro release of insulin from NCPs and ENCPs

A frequent problem associated with the formulation of drug-polymer nanocomplexes is the uncontrolled premature disassociation of the drug from the complexing polymer. In order to ensure the capacity of ENCPs to efficiently transfer the therapeutic payload from the intestinal cavity into the intestinal epithelium, we analyzed the behavior of the diblock PGA-PEG enveloped C12-r8-insulin formulation in SIF (pH 6.8) and FaSSIF-V2 (pH 6.5). As a control, we also analyzed the behavior of the non-enveloped NCPs, in order to elucidate the role of enveloping polymer in controlling the release of insulin. These two release media were selected in order to mimic the conditions of the intestinal fluids at different times, and to explore the effect of physiologically relevant bile salts and surfactants on the release profile of insulin from the carriers. As shown in Fig. 6, in the case of the non-enveloped NCPs, a certain amount of insulin was immediately released upon dilution of the NC suspension in simulated intestinal media (about 25% in SIF and 14% in FaSSIF-V2), however this premature release was reduced (< 10%) and no subsequent release was observed in the case of PGA-PEG enveloped ENCPs for up to 6 h (data not shown). We concluded that the enveloping polymer protected the ENCPs from a premature release upon contact with the intestinal fluids. In a second step, in order to understand the mechanism of release, we sought to simulate the release environment assuming that the ENCPs could enter the enterocytes *via* endocytosis and release their content at that level. This assumption is based on the reported fact that endocytosis is the predominant mechanism of uptake of nanoparticles with similar features (*i.e.* PGA-PEG coating and/or CPP complexation), followed by the endosomal pathway [59,60]. Along this pathway, the pH drops

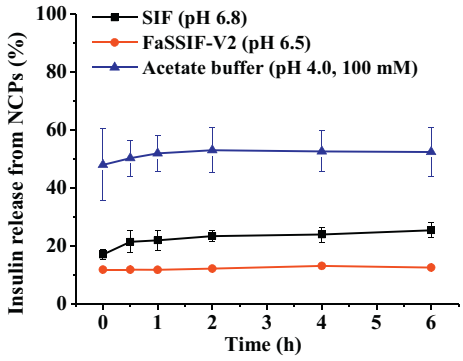

Fig. 6. Release profile of insulin from the non-enveloped C12-r8-insulin NCPs in SIF pH 6.8, FaSSIF-V2 pH 6.5 and acetate buffer pH 4.0 up to 6 h at 37 °C. Data are expressed as mean ± SD, n = 6.

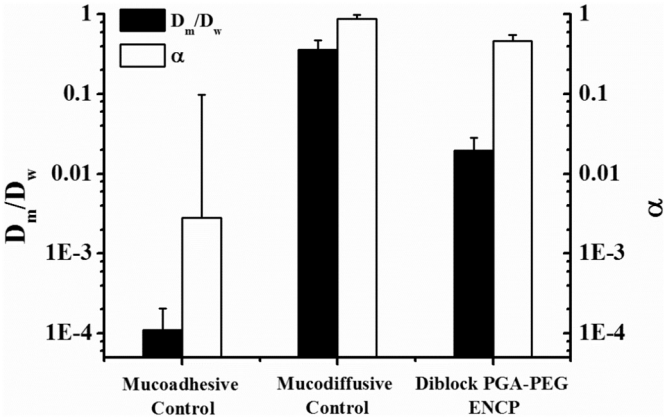

Fig. 7. Calculated D_m/D_w coefficients and α parameter of the diblock PGA-PEG enveloped ENCPs in porcine intestinal mucus at a time scale of 1 s (n ≥ 1000). Parameter α provides information about the nature of the diffusion of the nanoparticle in the mucus; free diffusive (α ~ 1); subdiffusive (0.2 < α < 0.9); immobile NPs (α < 0.2)).

sequentially, going from a pH of ~6.0 in early endosomes towards a more acidic pH that may reach a pH as low as 4.0. To understand the influence of this pH decline on drug release, we assessed the release of insulin from the C12-r8-insulin NCPs and the corresponding ENCPs in acetate buffer (pH 4.0, 100 mM). The results shown in Fig. 6 indicate that around 53% of the associated insulin was immediately released from NCPs in this acidic medium, whereas the release from the ENCPs was still very limited (< < 10%, data not shown). This pH-dependent release profile may be explained by the insulin decomplexation from C12-r8 at the low pH values. At pH 4.0, both insulin and C12-r8 become positively charged and, hence, electrostatically repulsed and released. Based on this *in vitro* release behavior, we could speculate that following oral administration, the PGA-PEG coating could not only preserve the stability of the ENCPs in the intestinal fluids, but also prevent the premature release of the peptide. This interpretation should be taken with caution, given the differences that exist between the *in vitro* conditions and the intracellular environment. In a realistic *in vivo* situation, it is possible that the drug release from ENCPs could be triggered by more sophisticated mechanisms.

3.7. Transport of PGA-PEG enveloped nanocomplexes (ENCPs) in intestinal mucus

Fig. 7 displays the diffusion capacity of the diblock PGA-PEG enveloped ENCPs, expressed as the effective diffusion coefficient in mucus (D_m) divided by D in water (D_m/D_w), as well as the α parameter at a sample time of 1 s. Fig. 7 also includes the results obtained with a mucoadhesive and a mucodiffusive control. The results indicate that the diblock PGA-PEG ENCPs present a moderate diffusion in mucus at 37 °C, with a mean α parameter value of 0.5 and a D_m/D_w ratio of 1.9×10^{-2}, which is one order of magnitude lower than the one obtained for the mucodiffusive control. These mucodiffusion values are in the same order of magnitude than those corresponding to the mucopenetrative PEG-PLGA NPs, with particle sizes varying between 90 nm of 164 nm, or PEG-polystyrene nanoparticles of 200 nm, when tested in human cervicovaginal mucus [61]. These acceptable mucodiffusive properties of ENCPs are justified by their almost neutral surface charge due to the presence of PEG chains on the ENCPs surface [35]. Overall, these results indicate the ability of the ENCPs to overcome the mucus barrier.

3.8. Cytotoxicity of ENCPs on Caco-2 cells

A concentration-dependent cytotoxicity profile (MTS assay) was observed for both, the diblock PGA-PEG enveloped ENCPs and the C12-

r8 control, upon incubation with Caco-2 cells for 2 h; while diblock PGA-PEG showed negligible cytotoxicity at the same concentrations (Fig. 8). Interestingly, the formation of ENCPs reduced the inherent cytotoxicity of the C12-r8, most probably due to the protective PGA-PEG shell. However, the reported toxicity studies of oligoarginines performed on rat intestinal tissues showed no toxicity [8]. Bearing these results in mind and the known capacity of r8 to enter the cells, it can be induced that the concentration-dependent cytotoxicity is directly associated to the permeation enhancement effect of CPP derivatives [62]. In conclusion, these results clearly show the positive contribution of the enveloping process in reducing the inherent toxicity of CPPs used as penetration enhancers.

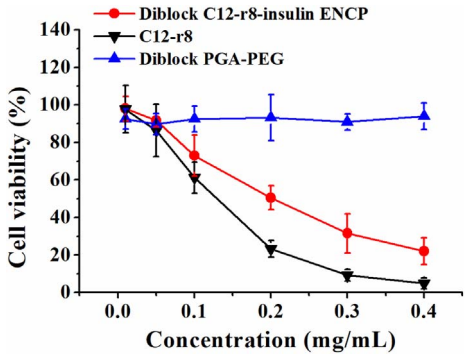

Fig. 8. Cell viability of the Caco-2 cell line after a 2 h incubation with: diblock PGA-PEG coated C12-r8-insulin, C12-r8, and diblock copolymer (Mean ± S.D., n = 9).

3.9. Effect on transepithelial electrical resistance (TEER) of Caco-2 cells

Although r8 is not supposed to affect the intercellular junctions, the limited information about the interaction of the CPP hydrophobic derivatives with the intestinal epithelium led us to investigate the potential interference of the C12 derivative with the intercellular junctions [62,63]. For this, we evaluated the TEER of the Caco-2 monolayer after exposure to the C12-r8- insulin nanocomplexes (NCPs) and the PGA-PEG enveloped nanocomplexes (ENCPs), at different concentrations (0.01 mg/mL (non-toxic), 0.05 mg/mL (non-toxic) and 0.2 mg/mL (50% decrease in cell viability)). A physical mixture of r8 and insulin was used as a control formulation. Simultaneously, Lucifer yellow (LY) was co-incubated with the formulations to visualize their effect on the paracellular transport. The results presented in Fig. 9A–C indicated that the TEER values were unaffected by the nanocomplexes irrespective of their composition and concentration. Similarly, no alteration in the monolayer was observed upon exposure to the physical mixture. In agreement with this, we observed that the apparent permeability values (Papp) of LY across the Caco-2 cell monolayer was not influenced by the previous exposure to the NCPs and ENCPs (Fig. 9D). These results confirmed that, at the concentration tested, C12-r8 did not interfere with the intercellular tight junctions.

3.10. Interaction of ENCPs with Caco-2 cells

In order to assess the possible value of the ENCPs technology as intracellular peptide delivery carriers, we studied the mechanism of interaction of FITC-labelled nanocarriers (diblock PGA-PEG) (0.2 mg/mL) with the Caco-2 cells for up to 2 h. The graphic representation of the flow cytometry analysis (Fig. 10A) shows a significant displacement of the fluorescence intensity peak corresponding to the cells treated with ENCPs. This displacement, which indicates that the number of positive cells is higher than 99%, is a clear indication of the important interaction of the ENCPs with the Caco-2 cells. These results were confirmed by confocal laser scanning microscopy (CLSM). The images presented in Fig. 10B show that FITC-labelled ENCPs (green) had a strong interaction with the Caco-2 monolayer and remained associated to it rather than being transported across it. Whether the ENCPs crossed the membrane and remain retained near the inner side of membrane or were simply adsorbed onto the membrane could not be discriminated from the visual observation of these images. To further clarify this behavior, we studied the interaction of the ENCPs with individual Caco-2 cells. In this situation the high internalization of the FITC-labelled ENCPs (green) could be easily visualized and presented in Fig. 10C.

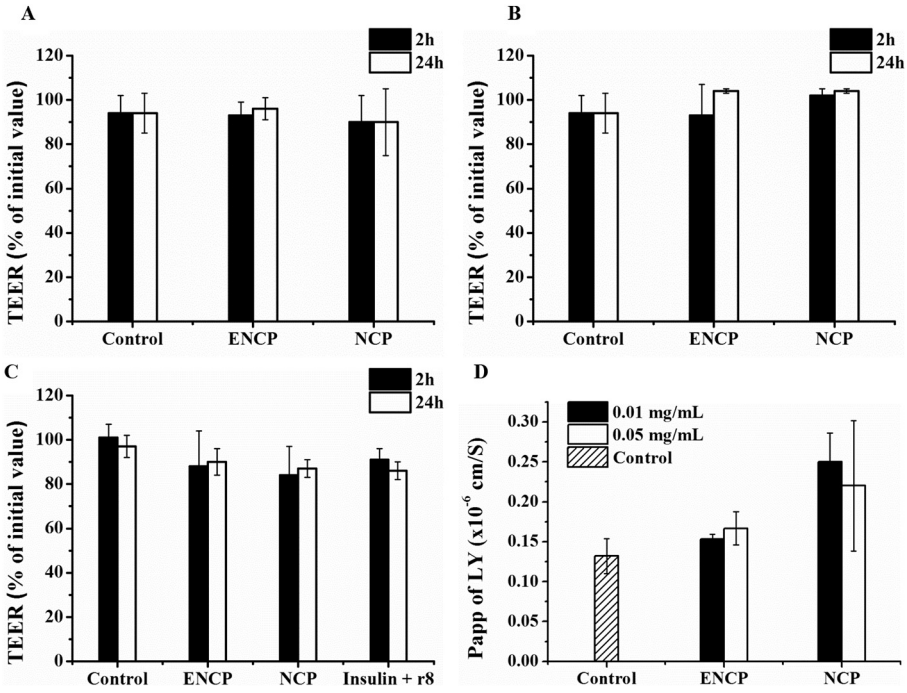

Fig. 9. TEER values of Caco-2 cell monolayers after a 2-h and 24-h exposure times to non-enveloped NCPs and diblock PGA-PEG ENCPs at different concentrations: (A) 0.01 mg/mL, (B) 0.05 mg/mL and (C) 0.2 mg/mL; and (D) Lucifer Yellow transport across Caco-2 cell monolayers after a-2 h exposure to different concentrations of NCP and ENCPs. Data is expressed as mean ± SD, n = 3, changes are considered statistically significant at $p < 0.05$.

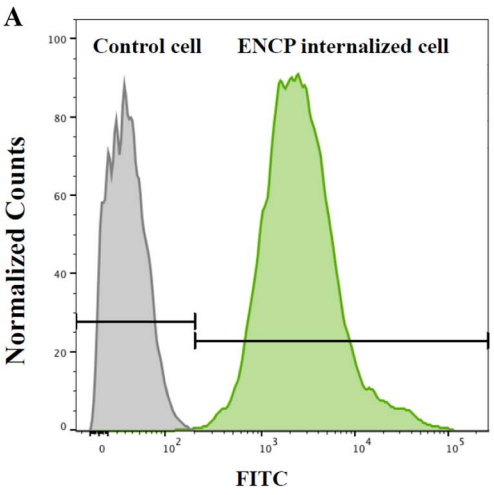

	FITC positive cells (% of parent)
Control	1.7 ± 4.5
ENCP treated	99.5 ± 0.6

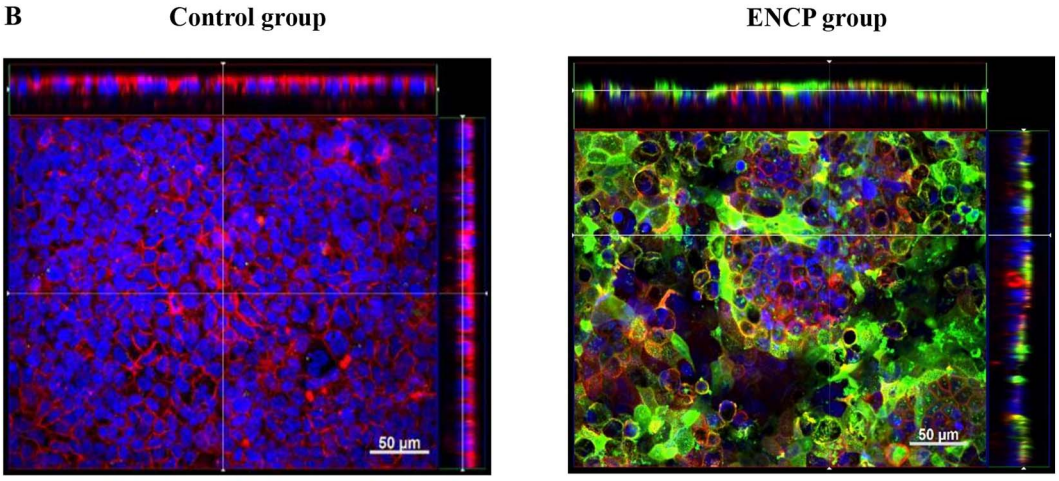

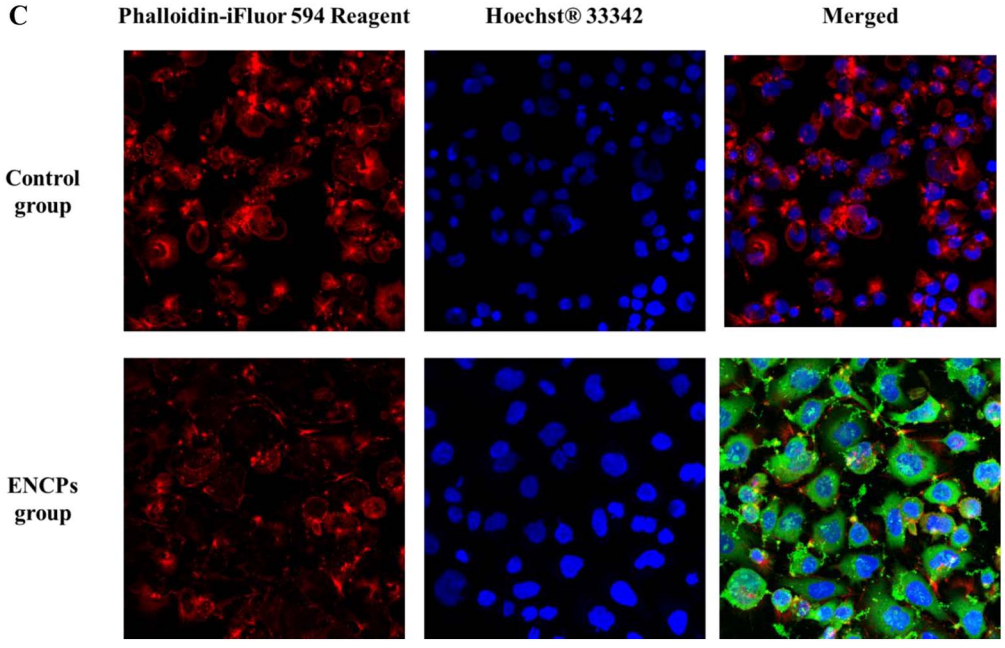

Fig. 10. (A) The Flow cytometry profile shows the fluorescence peaks corresponding to the Caco-2 cells that internalized the fluorescent ENCPs (0.2 mg/mL) after a 2-hr incubation time (peak to the right) and the non-fluorescent control cells (peak to the left), n = 9. (B) CLSM images (y-z, x-y and x-z sections) of the cell membranes upon staining with Rhodamine-phalloidine (red color, F-actin) and DAPI (blue color, cell nuclei). (C) CLSM images of the Caco-2 cells upon staining with Phalloidin-iFluor 594 Reagent - CytoPainter (red color, F-actin) Hoechst® 33342 (blue color, cell nuclei). The FITC-labelled ENCPs are shown in green color (FITC). (For interpretation of the references to color in this figure legend, the reader is referred to the web version of this article.)

3.11. Quantitative cell uptake and transport of insulin

To evaluate the ability of ENCPs to transport insulin across the enterocytes, both the amount of insulin internalized by the cells and the amount transported into the basolateral compartment of the Caco-2 cells monolayer was quantitatively analyzed by LC/MS/MS. NCPs, ENCPs, as well as the physical mixture of r8 and insulin were tested at concentrations of 0.05 mg/mL and 0.2 mg/mL (or the equivalent concentration of insulin and r8 in the case of the controls). However, at the concentration of 0.05 mg/mL, insulin levels in the basolateral compartment, or inside the cell monolayers, were below the detection limit of the LC/MS/MS technique, so we proceeded testing at the concentration of 0.2 mg/mL. The results in Fig. 11A and B, show a very low insulin internalization into the Caco-2 monolayer when mixed with r8. This observation is in line with the report by Kamei et al. who described that the visible precipitation of CPPs and insulin compromised the enhancement of insulin absorption on rats' ileal tissues [9]. In contrast, a dramatically high insulin internalization was observed when administered associated to NCPs (79.37 ± 3.41%) or PGA-PEG ENCPs (47.59 ± 5.79%) (Fig. 11A). However, this high internalization was not translated into a subsequent insulin transport. In fact, the highest value, which was observed for the ENCPs enveloped with diblock PGA-PEG (Fig. 11B) was only 2.11 ± 0.33%. The greater insulin uptake achieved for the NCPs as compared to that of ENCPs could be simply understood by the more important internalization capacity of cationic nanoparticles *vs.* the neutral PEGylated ones. However, we should keep in mind that the NCPs are neither stable in the intestinal fluids nor able to diffuse across the mucus and, therefore, their high internalization capacity would not be translated in an *in vivo* situation, in the presence of enzymes and mucus. Irrespective of the differences between the enveloped and non-enveloped nanocarriers, a clear conclusion from this study is that the ENCPs are highly efficient as intracellular drug delivery carriers, reaching the highest intracellular peptide delivery ever reported (47.59%) in the Caco-2 model, however, their capacity to facilitate the trans-epithelial transport appears to be limited.

3.12. In vivo biodistribution of radiolabelled PGA-PEG enveloped nanocomplexes (ENCPs)

Diblock PGA-PEG coated ENCPs were successfully labelled with Technetium-99m (^{99m}Tc) (99% labeling efficiency according to paper chromatography analysis) (Fig. S6). The radiolabelled ENCPs exhibited similar particle size as the non-labelled ENCPs and remained stable after incubation in SGF for 2 h and in SIF for 4 h (Fig. S7). No significant release of the radioisotope was observed under the same conditions. Fig. 12A shows SPECT-CT images of the distribution of the radiolabelled ENCPs, following their oral administration to rats. The results indicate that the ENCPs traveled along the gastric cavity and small intestine (duodenum, jejunum and ileum) for 2–4 h and they accumulated at the cecum level for at least 11 h. Curiously, only a small amount was accumulated in the colonic region. On the contrary, as observed in Fig. 12B, the free radioisotope (control) was found mostly in the stomach and was eliminated from the GIT more rapidly than the ENCPs (Fig. 12D). Not unexpectedly, the amount of radioactivity recovered in GIT for control group was between 60 and 80%, as a result of the fast accumulation in the bladder and subsequent excretion of the radiomarker. In the case of ENCPs, over 90% radioactivity recovery was observed with an accumulation in the bladder only at 11 h post-administration. This retarded excretion of the marker was attributed to its attachment to the nanocarrier and its accumulation at the intestinal level. Indeed, these results indicate that the ENCPs did not adhere to gastric mucus but exhibited a significant and prolonged interaction with the intestinal mucosa, particularly high at the cecum region. This specific accumulation at the cecum region has been previously reported by other groups [18,64,65], and it has been attributed to the physiology of the rat intestine. In fact, the cecum of rodent species is extremely large and adapted to their nutrition needs [66,67]. Overall, these data highlight the specific accumulation of the ENCPs in the intestinal mucosa, a result that is in agreement with their high internalization by the Caco-2 monolayers.

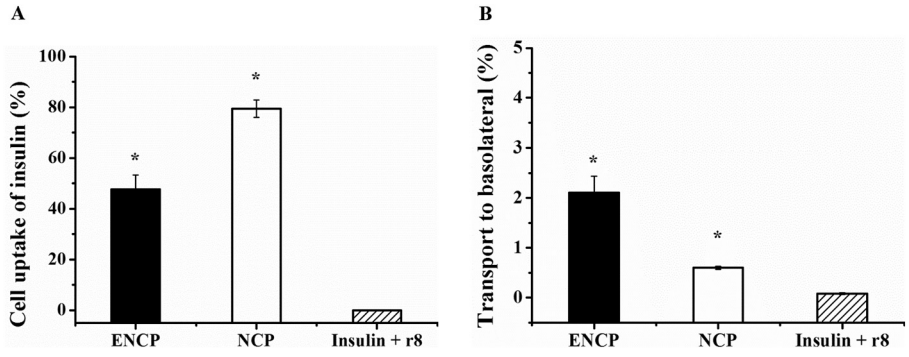

Fig. 11. (A) Cell uptake and (B) apical to basolateral transport of insulin across the Caco-2 cell monolayer with 0.2 mg/mL of ENCPs, NCPs or a physical mixture of r8 and insulin at 37 °C after a 2 h incubation. Data are expressed as mean ± SD, n = 3. Changes are considered statistically significant at $p < 0.05$.

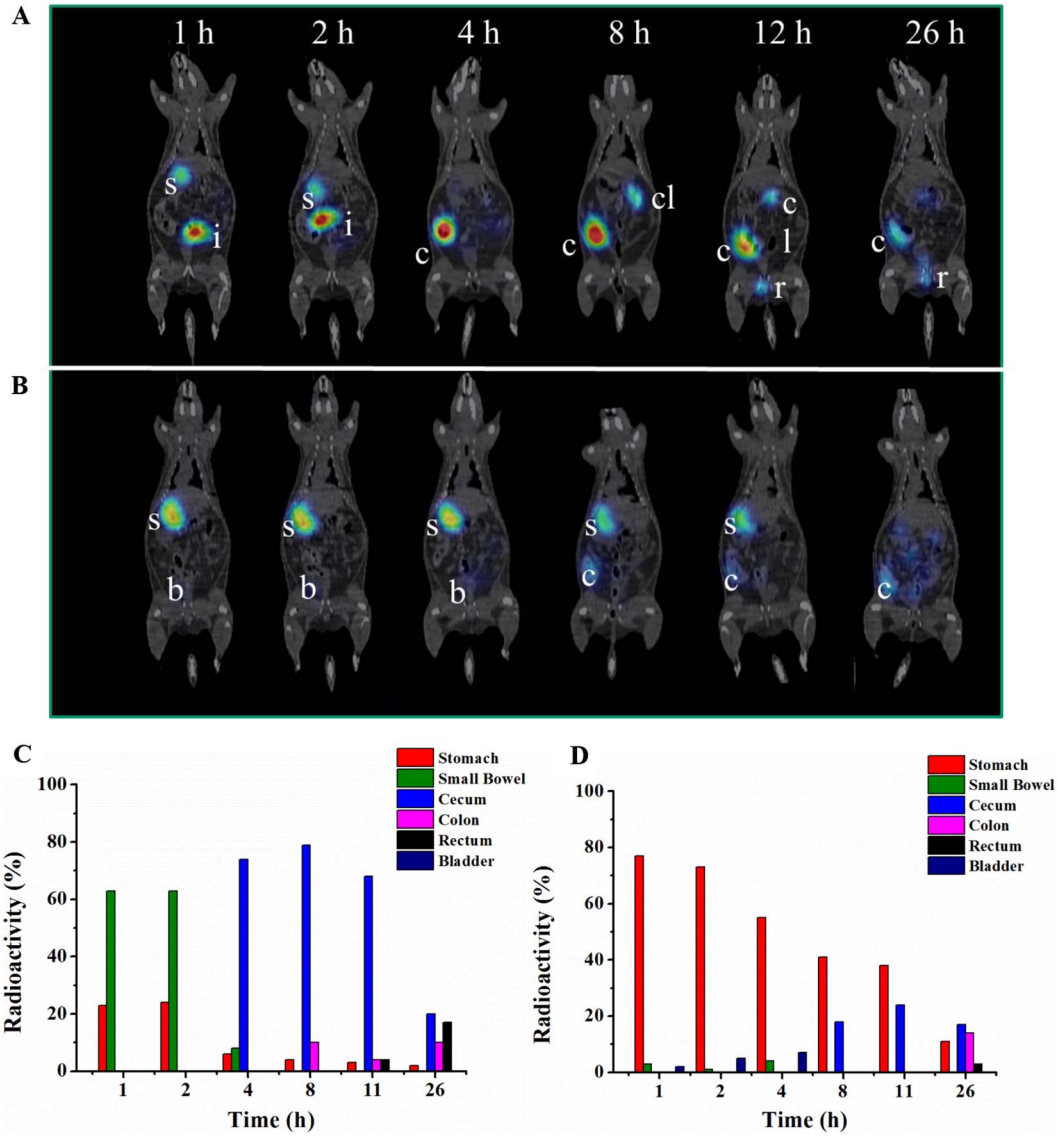

Fig. 12. SPECT-CT images following the oral biodistribution of (A) ^{99m}Tc-ENCPs and (B) the free ^{99m}Tc (control) at 1, 2, 4, 8, 11 and 26 h. Biodistribution of (C) ^{99m}Tc-ENCP and (D) free ^{99m}Tc (control) in Wistar rats with time. (s = stomach; i = intestine (duodenum, jejunum and ileum); c = cecum; cl = colon; r = rectum; b = bladder).

3.13. *In vivo* response to insulin-loaded ENCPs

Following the observed accumulation of ENCPs at the intestinal level, we assessed whether this would be translated into an enhanced systemic absorption of the associated peptide. As a simple way to estimate the absorption of insulin, we monitored the blood glucose levels after administration of the formulation in healthy rats in a realistic condition, *i.e.* oral administration (50 IU/kg) of the freeze-dried ENCPs powder introduced in an enteric mini-capsule. This enteric capsule, which starts dissolving at pH 6, was used to facilitate the delivery of the ENCPs free at the intestinal level. Fig. 13 indicates that, overall, with the exception of one point (2 h), there are not statistically significant differences between the rat glucose levels observed for the insulin and for the ENCP formulation. The comparison of these *in vivo* data with those obtained *in vitro* (stability, mucodiffusion behavior and capacity to enter the Caco-2 cells) led us to speculate about the potential reason behind the lack of correlation. Based on the extraordinary uptake of the diblock PGA-PEG enveloped ENCPs by the Caco-2 cells and the very high insulin retention (47.59%), we have formulated the hypothesis that ENCPs were internalized in the intestinal epithelium where they formed a depot reservoir from which insulin might be slowly released.

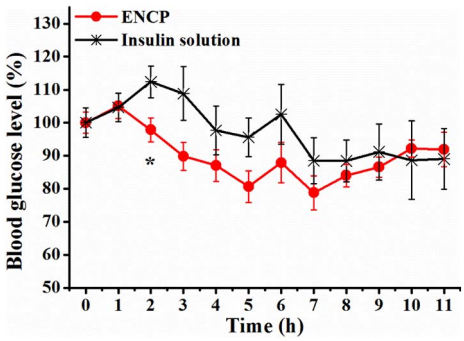

Fig. 13. Standardized hypoglycemic effect in healthy rats following oral administration of insulin-loaded ENCPs or plain insulin in enteric capsule (50 IU/kg). Data represents the mean ± S.E., n = 8. Differences were considered statistically significant at *p < 0.05.

In fact, the limited insulin transport (2.11%), observed in the Caco-2 model would be in agreement with the mild systemic drug effect. Restricted by the peptide drug model selected in this work, unfortunately, it was not possible to visualize a potential benefit of the formulation for

a local therapeutic effect. However, the high insulin internalization by the enterocytes led us to speculate about the potential utility of the ENCPs for the intestinal delivery of locally acting peptides. Current studies are aimed at validating this hypothesis.

4. Conclusion

Herein, we describe the development and characterization of a new oral peptide delivery system based on the complexation of the peptide with hydrophobized CPPs (C12-r8) and subsequent envelopment by a protective layer made of PEGylated polyaminoacids (PGA-PEG), named as ENPCs. The system was stable in the intestinal fluids and provided adequate protection to the associated model peptide - insulin - from degradation. In addition, the system showed a capacity to diffuse through intestinal mucus and transport insulin into the Caco-2 monolayer in a very efficient manner, reaching the highest *in vitro* insulin uptake ever reported (47.59 ± 5.79%). This important retention in the enterocytes, which was corroborated in the *in vivo* biodistribution studies, was not, however, translated into an enhanced systemic absorption. These results suggest the potential value of the ENCPs for the local delivery of peptide drugs to the intestinal mucosa. Current studies are aimed to validate this hypothesis.

Acknowledgements

The work was supported by the European TRANS-INT Consortium, which received funding from the European Union's Seventh Framework Programme for research, technological development and demonstration under grant agreement No. 281035.

Appendix A. Supplementary data

Supplementary data to this article can be found online at https://doi.org/10.1016/j.jconrel.2018.03.004.

References

[1] K. Fosgerau, T. Hoffmann, Peptide therapeutics: current status and future directions, Drug Discov. Today 20 (2015) 122–128.
[2] M.L. Smythe, Orally delivered peptides for treatment of inflammatory bowel disease, Reference Module in Chemistry, Molecular Sciences and Chemical Engineering, Elsevier, 2016.
[3] A. Beloqui, A. des Rieux, V. Préat, Mechanisms of transport of polymeric and lipidic nanoparticles across the intestinal barrier, Adv. Drug Deliv. Rev. 106 (2016) 242–255.
[4] H. Malhaire, J.-C. Gimel, E. Roger, J.-P. Benoît, F. Lagarce, How to design the surface of peptide-loaded nanoparticles for efficient oral bioavailability? Adv. Drug Deliv. Rev. 106 (2016) 320–336.
[5] Z. Niu, I. Conejos-Sánchez, B.T. Griffin, C.M. O'Driscoll, M.J. Alonso, Lipid-based nanocarriers for oral peptide delivery, Adv. Drug Deliv. Rev. 106 (2016) 337–354.
[6] T.A.S. Aguirre, D. Teijeiro-Osorio, M. Rosa, I.S. Coulter, M.J. Alonso, D.J. Brayden, Current status of selected oral peptide technologies in advanced preclinical development and in clinical trials, Adv. Drug Deliv. Rev. 106 (2016) 223–241.
[7] M. Sánchez-Navarro, J. Garcia, E. Giralt, M. Teixidó, Using peptides to increase transport across the intestinal barrier, Adv. Drug Deliv. Rev. 106 (2016) 355–366.
[8] M. Morishita, N. Kamei, J. Ehara, K. Isowa, K. Takayama, A novel approach using functional peptides for efficient intestinal absorption of insulin, J. Control. Release 118 (2007) 177–184.
[9] N. Kamei, M. Morishita, Y. Eda, N. Ida, R. Nishio, K. Takayama, Usefulness of cell-penetrating peptides to improve intestinal insulin absorption, J. Control. Release 132 (2008) 21–25.
[10] C. Damgé, C. Michel, M. Aprahamian, P. Couvreur, New approach for oral administration of insulin with polyalkylcyanoacrylate nanocapsules as drug carrier, Diabetes 37 (1988) 246–251.
[11] C. Damgé, C. Michel, M. Aprahamian, P. Couvreur, J.P. Devissaguet, Nanocapsules as carriers for oral peptide delivery, J. Control. Release 13 (1990) 233–239.
[12] A.K. Agrawal, H. Harde, K. Thanki, S. Jain, Improved stability and antidiabetic potential of insulin containing folic acid functionalized polymer stabilized multilayered liposomes following oral administration, Biomacromolecules 15 (2014) 350–360.
[13] H. Takeuchi, Y. Matsui, H. Yamamoto, Y. Kawashima, Mucoadhesive properties of carbopol or chitosan-coated liposomes and their effectiveness in the oral administration of calcitonin to rats, J. Control. Release 86 (2003) 235–242.
[14] F. Araujo, N. Shrestha, M.A. Shahbazi, P. Fonte, E.M. Makila, J.J. Salonen, J.T. Hirvonen, P.L. Granja, H.A. Santos, B. Sarmento, The impact of nanoparticles on the mucosal translocation and transport of GLP-1 across the intestinal epithelium, Biomaterials 35 (2014) 9199–9207.
[15] C. Prego, M. García, D. Torres, M.J. Alonso, Transmucosal macromolecular drug delivery, J. Control. Release 101 (2005) 151–162.
[16] C. Prego, M. Fabre, D. Torres, M. Alonso, Efficacy and mechanism of action of chitosan nanocapsules for oral peptide delivery, Pharm. Res. 23 (2006) 549–556.
[17] E.-Y. Chuang, G.T.H. Nguyen, F.-Y. Su, K.-J. Lin, C.-T. Chen, F.-L. Mi, T.-C. Yen, J.-H. Juang, H.-W. Sung, Combination therapy via oral co-administration of insulin- and exendin-4-loaded nanoparticles to treat type 2 diabetic rats undergoing OGTT, Biomaterials 34 (2013) 7994–8001.
[18] K. Sonaje, K.-J. Lin, S.-P. Wey, C.-K. Lin, T.-H. Yeh, H.-N. Nguyen, C.-W. Hsu, T.-C. Yen, J.-H. Juang, H.-W. Sung, Biodistribution, pharmacodynamics and pharmacokinetics of insulin analogues in a rat model: oral delivery using pH-responsive nanoparticles vs. subcutaneous injection, Biomaterials 31 (2010) 6849–6858.
[19] S. Jain, V.V. Rathi, A.K. Jain, M. Das, C. Godugu, Folate-decorated PLGA nanoparticles as a rationally designed vehicle for the oral delivery of insulin, Nanomedicine 7 (2012) 1311–1337.
[20] M.J. Santander-Ortega, D. Bastos-González, J.L. Ortega-Vinuesa, M.J. Alonso, Insulin-loaded PLGA nanoparticles for oral administration: an in vitro physicochemical characterization, J. Biomed. Nanotechnol. 5 (2009) 45–53.
[21] F.-d. Cui, A.-j. Tao, D.-m. Cun, L.-q. Zhang, K. Shi, Preparation of insulin loaded PLGA-Hp55 nanoparticles for oral delivery, J. Pharm. Sci. 96 (2007) 421–427.
[22] A.C. Foss, T. Goto, M. Morishita, N.A. Peppas, Development of acrylic-based copolymers for oral insulin delivery, Eur. J. Pharm. Biopharm. 57 (2004) 163–169.
[23] M. Morishita, T. Goto, N.A. Peppas, J.I. Joseph, M.C. Torjman, C. Munsick, K. Nakamura, T. Yamagata, K. Takayama, A.M. Lowman, Mucosal insulin delivery systems based on complexation polymer hydrogels: effect of particle size on insulin enteral absorption, J. Control. Release 97 (2004) 115–124.
[24] W. Leobandung, H. Ichikawa, Y. Fukumori, N.A. Peppas, Preparation of stable insulin-loaded nanospheres of poly(ethylene glycol) macromers and N-isopropyl acrylamide, J. Control. Release 80 (2002) 357–363.
[25] C. Chen, T. Fan, Y. Jin, Z. Zhou, Y. Yang, X. Zhu, Z.-r. Zhang, Q. Zhang, Y. Huang, Orally delivered salmon calcitonin-loaded solid lipid nanoparticles prepared by micelle–double emulsion method via the combined use of different solid lipids, Nanomedicine 8 (2012) 1085–1100.
[26] B. Sarmento, S. Martins, D. Ferreira, E.B. Souto, Oral insulin delivery by means of solid lipid nanoparticles, Int. J. Nanomedicine 2 (2007) 743–749.
[27] A. Viscido, A. Capannolo, G. Latella, R. Caprilli, G. Frieri, Nanotechnology in the treatment of inflammatory bowel diseases, J. Crohn's Colitis 8 (2014) 903–918.
[28] S. Hua, E. Marks, J.J. Schneider, S. Keely, Advances in oral nano-delivery systems for colon targeted drug delivery in inflammatory bowel disease: selective targeting to diseased versus healthy tissue, Nanomedicine 11 (2015) 1117–1132.
[29] A. Lamprecht, Nanomedicines in gastroenterology and hepatology, Nat. Rev. Gastroenterol. Hepatol. 12 (2015) 195–204.
[30] G. Fuhrmann, J.-C. Leroux, Improving the stability and activity of oral therapeutic enzymes—recent advances and perspectives, Pharm. Res. 31 (2014) 1099–1105.
[31] A.N. Zelikin, C. Ehrhardt, A.M. Healy, Materials and methods for delivery of biological drugs, Nat. Chem. 8 (2016) 997–1007.
[32] S. Mitragotri, P.A. Burke, R. Langer, Overcoming the challenges in administering biopharmaceuticals: formulation and delivery strategies, Nat. Rev. Drug Discov. 13 (2014) 655–672.
[33] M. Tobio, A. Sanchez, I.S.A. Vila, C. Evora, J.L. Vila-Jato, M.J. Alonso, The role of PEG on the stability in digestive fluids and in vivo fate of PEG-PLA nanoparticles following oral administration, Colloids Surf. B: Biointerfaces 18 (2000) 315–323.
[34] L.M. Ensign, R. Cone, J. Hanes, Oral drug delivery with polymeric nanoparticles: the gastrointestinal mucus barriers, Adv. Drug Deliv. Rev. 64 (2012) 557–570.
[35] K. Maisel, L. Ensign, M. Reddy, R. Cone, J. Hanes, Effect of surface chemistry on nanoparticle interaction with gastrointestinal mucus and distribution in the gastrointestinal tract following oral and rectal administration in the mouse, J. Control. Release 197 (2015) 48–57.
[36] S.K. Lai, D.E. O'Hanlon, S. Harrold, S.T. Man, Y.-Y. Wang, R. Cone, J. Hanes, Rapid transport of large polymeric nanoparticles in fresh undiluted human mucus, Proc. Natl. Acad. Sci. 104 (2007) 1482–1487.
[37] H.E. Lee, M.J. Lee, C.R. Park, A.Y. Kim, K.H. Chun, H.J. Hwang, D.H. Oh, S.O. Jeon, J.S. Kang, T.S. Jung, G.J. Choi, S. Lee, Preparation and characterization of salmon calcitonin-sodium triphosphate ionic complex for oral delivery, J. Control. Rel. 143 (2010) 251–257.
[38] S. Sun, N. Liang, H. Piao, H. Yamamoto, Y. Kawashima, F. Cui, Insulin-S.O (sodium oleate) complex-loaded PLGA nanoparticles: formulation, characterization and in vivo evaluation, J. Microencapsul. 27 (2010) 471–478.
[39] M.J. Santander-Ortega, M. de la Fuente, M.V. Lozano, M.E. Bekheet, F. Progatzky, A. Elouzi, I.F. Uchegbu, A.G. Schatzlein, Hydration forces as a tool for the optimization of core-shell nanoparticle vectors for cancer gene therapy, Soft Matter 8 (2012) 12080–12092.
[40] N. Kamei, M. Morishita, Y. Kanayama, K. Hasegawa, M. Nishimura, E. Hayashinaka, Y. Wada, Y. Watanabe, K. Takayama, Molecular imaging analysis of intestinal insulin absorption boosted by cell-penetrating peptides by using positron emission tomography, J. Control. Rel. 146 (2010) 16–22.
[41] E. Jantratid, N. Janssen, C. Reppas, J.B. Dressman, Dissolution media simulating conditions in the proximal human gastrointestinal tract: an update, Pharm. Res. 25 (2008) 1663–1676.
[42] Z. Niu, E. Tedesco, F. Benetti, A. Mabondzo, I.M. Montagner, I. Marigo, D. Gonzalez-Touceda, S. Tovar, C. Diéguez, M.J. Santander-Ortega, M.J. Alonso, Rational design of polyarginine nanocapsules intended to help peptides overcoming intestinal barriers, J. Control. Release 263 (2017) 4–17.

[43] M.J. Santander-Ortega, M. Plaza-Oliver, V. Rodriguez-Robledo, L. Castro-Vazquez, N. Villaseca-Gonzalez, J. Gonzalez-Fuentes, E.L. Cano, P. Marcos, M.V. Lozano, M.M. Arroyo-Jimenez, PEGylated nanoemulsions for oral delivery: role of the inner core on the final fate of the formulation, Langmuir 33 (2017) 4269–4279.
[44] J. Suh, M. Dawson, J. Hanes, Real-time multiple-particle tracking: applications to drug and gene delivery, Adv. Drug Deliv. Rev. 57 (2005) 63–78.
[45] E. Zagato, K. Forier, T. Martens, K. Neyts, J. Demeester, S. De Smedt, K. Remaut, K. Braeckmans, Single-particle tracking for studying nanomaterial dynamics: applications and fundamentals in drug delivery, Nanomedicine 9 (2014) 913–927.
[46] Y.Y. Wang, S.K. Lai, J.S. Suk, A. Pace, R. Cone, J. Hanes, Addressing the PEG mucoadhesivity paradox to engineer nanoparticles that "slip" through the human mucus barrier, Angew. Chem. Int. Ed. Engl. 47 (2008) 9726–9729.
[47] T. Yu, Y.-Y. Wang, M. Yang, C. Schneider, W. Zhong, S. Pulicare, W.-J. Choi, O. Mert, J. Fu, S.K. Lai, J. Hanes, Biodegradable mucus-penetrating nanoparticles composed of diblock copolymers of polyethylene glycol and poly(lactic-co-glycolic acid), Drug Deliv. Trans. Res. 2 (2012) 124–128.
[48] L. Inchaurraga, N. Martín-Arbella, V. Zabaleta, G. Quincoces, I. Peñuelas, J.M. Irache, In vivo study of the mucus-permeating properties of PEG-coated nanoparticles following oral administration, Eur. J. Pharm. Biopharm. 97 (2015) 280–289.
[49] E.-S. Khafagy, N. Kamei, M. Takeda-Morishita, Cell-penetrating peptide-biodrug strategy for oral and nasal delivery: review of recent findings, J. Exp. Clin. Med. 4 (2012) 198–202.
[50] N. Kamei, M. Morishita, K. Takayama, Importance of intermolecular interaction on the improvement of intestinal therapeutic peptide/protein absorption using cell-penetrating peptides, J. Control. Rel. 136 (2009) 179–186.
[51] M.J. Santander-Ortega, M. de la Fuente, M.V. Lozano, M.L. Tsui, K. Bolton, I.F. Uchegbu, A.G. Schatzlein, Optimisation of synthetic vector systems for cancer gene therapy - the role of the excess of cationic dendrimer under physiological conditions, Curr. Top. Med. Chem. 14 (2014) 1172–1181.
[52] Z.-H. Zhang, Y.-L. Zhang, J.-P. Zhou, H.-X. Lv, Solid lipid nanoparticles modified with stearic acid-octaarginine for oral administration of insulin, Int. J. Nanomedicine 7 (2012) 3333–3339.
[53] U. Koppelhus, T. Shiraishi, V. Zachar, S. Pankratova, P.E. Nielsen, Improved cellular activity of antisense peptide nucleic acids by conjugation to a cationic peptide-lipid (CatLip) domain, Bioconjug. Chem. 19 (2008) 1526–1534.
[54] T. Shiraishi, P.E. Nielsen, Improved cellular uptake of antisense peptide nucleic acids by conjugation to a cell-penetrating peptide and a lipid domain, in: S.S. Mark (Ed.), Bioconjugation Protocols: Strategies and Methods, Humana Press, Totowa, NJ, 2011, pp. 209–221.
[55] Y. Li, Y. Li, X. Wang, R.J. Lee, L. Teng, Fatty acid modified octa-arginine for delivery of siRNA, Int. J. Pharm. 495 (2015) 527–535.
[56] L. Tonges, P. Lingor, R. Egle, G.P. Dietz, A. Fahr, M. Bahr, Stearylated octaarginine and artificial virus-like particles for transfection of siRNA into primary rat neurons, RNA 12 (2006) 1431–1438.
[57] M. Garcia-Fuentes, C. Prego, D. Torres, M.J. Alonso, A comparative study of the potential of solid triglyceride nanostructures coated with chitosan or poly(ethylene glycol) as carriers for oral calcitonin delivery, Eur. J. Pharm. Sci. 25 (2005) 133–143.
[58] M.J. Santander-Ortega, N. Csaba, L. González, D. Bastos-González, J.L. Ortega-Vinuesa, M.J. Alonso, Protein-loaded PLGA–PEO blend nanoparticles: encapsulation, release and degradation characteristics, Colloid Polym. Sci. 288 (2009) 141–150.
[59] B.R. Liu, S.-Y. Lo, C.-C. Liu, C.-L. Chyan, Y.-W. Huang, R.S. Aronstam, H.-J. Lee, Endocytic trafficking of nanoparticles delivered by cell-penetrating peptides comprised of Nona-arginine and a penetration accelerating sequence, PLoS One 8 (2013) e67100.
[60] S. Lukasiewicz, K. Szczepanowicz, E. Blasiak, M. Dziedzicka-Wasylewska, Biocompatible polymeric nanoparticles as promising candidates for drug delivery, Langmuir 31 (2015) 6415–6425.
[61] Q. Xu, N.J. Boylan, S. Cai, B. Miao, H. Patel, J. Hanes, Scalable method to produce biodegradable nanoparticles that rapidly penetrate human mucus, J. Control. Rel. 170 (2013) 279–286.
[62] D.R. Thakker, P.D. Ward, Compositions and methods for enhancing paracellular permeability across epithelial and endothelial barriers, in, US Patent, 2010.
[63] K.I. Cumming, Z. Ramtoola, Solid oral dosage form containing an enhancer, in, US Patent, 2010.
[64] A.T. Florence, N. Hussain, Transcytosis of nanoparticle and dendrimer delivery systems: evolving vistas, Adv. Drug Deliv. Rev. 50 (2001) S69–S89.
[65] F. Varga, Transit time changes with age in the gastrointestinal tract of the rat, Digestion 14 (1976) 319–324.
[66] J.M. DeSesso, C.F. Jacobson, Anatomical and physiological parameters affecting gastrointestinal absorption in humans and rats, Food Chem. Toxicol. 39 (2001) 209–228.
[67] J.M. DeSesso, A.L. Williams, Contrasting the gastrointestinal tracts of mammals: factors that influence absorption, Ann. Rep. Med. Chem. 43 (2008) 353–371.